Experiments and computations on steel bridge corroded beam ends

George Tzortzinis[1], Brendan T. Knickle[2], Simos Gerasimidis[3], Alexander Bardow[4], Sergio F. Breña[5]

Abstract
According to recent estimates the number of deficient bridges in the USA is more than 50,000 and the rehabilitation of these structures is considered an enormous task. A common cause of deterioration of steel bridges in the Northern part of the country is the leaking water which develops after the use of de-icing mixtures on the bridges. The corrosion appears almost always at the ends of steel girders above the bearing leading to a reduction of strength. There have been several recorded cases where the phenomenon is extensive and the bridge has to be closed for safety reasons. This research focuses on unstiffened deteriorated steel girder bridges and aims to develop a new procedure to accurately evaluate their remaining strength. First, two loading tests are conducted to investigate the effect of thickness reduction on girders' capacity. The tested girders were removed from an in-service bridge, the need for artificial corrosion was precluded. Second, the experimentally obtained capacities are used to evaluate the current MassDOT procedures for beams with deteriorated ends. Finally, analytical procedure is developed to determine the impact of corrosion on the beams' capacity. The whole girder along with the bearing is simulated, and the model is calibrated using the experimental data. New procedures are expected to be based on this study, which could be incorporated in Bridge Manuals across the country.

1. Introduction
According to the Federal Highway Administration in 2017 (FHWA 2017a), the State of Massachusetts maintained 5,192 bridges, of which 482 have been characterized as structurally deficient. The same ratio (9%) is representative for the entire US, which maintains a total of more than 600,000 bridges (FHWA 2017a). It is worth mentioning that from the 54,560 deficient bridges, 43% were built 69 to 118 or more years ago based on the National Bridge Inventory Database (FHWA 2017b), while the design service life is 75 years (AASHTO 2012). According to the American Society of Civil Engineers (ASCE), requirements for the nation's bridge rehabilitations approach the amount of $123 billion (ASCE 2017). Considering that more than

---

[1] Graduate Research Assistant, University of Massachusetts Amherst, <gtzortzinis@umass.edu>
[2] Graduate Research Assistant, University of Massachusetts Amherst, <bknickle@umass.edu>
[3] Assistant Professor, University of Massachusetts Amherst, <sgerasimidis@umass.edu>
[4] State Bridge Engineer, Massachusetts Department of Transportation, <alexander.bardow@state.ma.us>
[5] Professor, University of Massachusetts Amherst, <brena@umass.edu>

188 million trips are taken every day across structurally deficient bridges (ASCE 2017) regulations are necessary to ensure safety.

A bridge can be characterised as structurally deficient if at least one of its components has a condition rating of poor or worse. The critical components are the deck, superstructure and substructure or culvert. Corrosion damage, which affects mainly the superstructure, results in $8.3 billion in annual expenses for repairs or bridge replacement in the US alone (Koch et al. 2002). Inspection engineers are increasingly witnessing instances of deterioration of the web at steel beams ends due to corrosion mainly because of leaking bridge joints. This phenomenon is more intense in the northern parts of the country, because the leaking water contains high concentration of chemicals and salt due to winterizing procedures during the heavy winters. Frequently this deterioration occurs at a critical region where the beam is supported on its bearing, which leads to a significant reduction in the load carrying capacity of the beam. In extreme cases, the deteriorated web fails and the bridge has to be closed.

Over time, the damaging phenomenon has attracted the interest of engineers and researchers. During the last decades, some efforts have been carried out in an attempt to determine the remaining capacity of corroded beam ends. Researches have followed both experimental and computational approaches. One of the earliest efforts on the reduction in capacity for deteriorating steel bridges was performed by Kayser et al. (1989) who developed a corrosion damage model while determining the load-carrying capacity of the girder in bending, shear and bearing. Van de Lindt et al. (2013) conducted experimental and analytical work on beams 3 feet in length, with artificial web and flange thickness reduction above the bearing. Outside the US, efforts to study the phenomenon with computational and experimental work have been conducted and reported from Japan and Korea. Sugimoto et al. (2006) tested an actual deck plate girder constructed in the beginning of twentieth century, in an effort to evaluate the durability of railway steel bridges. Liu et al. (2011) investigated the impact of corrosion height and thickness reduction of steel girders with stiffeners. Ahn et al. (2013a) pointed out that the pattern's shape (rectangular or triangular) affects the capacity only when it intersects with the tension field of the web panel. The same research group performed experiments on stiffened beams with artificial corrosion thickness reduction (Kim et al. 2013) and pitting holes (Ahn et al. 2015). They also proposed a method for residual shear strength evaluation of web corroded panels (Ahn et al. 2013b). Usukura et al. (2013) conducted computational parametric analysis in order to investigate the capacity and the collapse mechanism of stiffened corroded girder ends. Yamaghuchi et al. (2013) identified the significance of the corrosion pattern effect on the load-carrying capacity of deteriorated beams. The challenge of non-uniform local corrosion damage was the focus of the study by Khurram et al. (2014) who indicated that the minimum thickness within any damage height may be used to simulate the corrosion damage in a computational analysis. A different approach was followed by Gheitasi et al. (2015). This research was not limited to the behavior of individual deteriorated components but tested the overall redundancy and operational safety of a bridge.

There is also a wide choice of repair techniques in the literature. Ahn et al. (2013c) proposed CFRP usage due to its low weight, high strength, and its rapid and simple application. Miyashita et al. (2015), using the same repairing method, conducted experimental and numerical shear buckling tests, reporting recovery of load carrying capacity. Ogami et al. (2015) attached studs

and rebar to the corroded girder before covering it with resin. With the proposed technique, buckling was prevented under axial compressive loading. Another method proposed by Zmetra et al. (2017) is to encase the corroded region with ultrahigh- performance concrete (UHPC). UHPC implementation managed to restore the capacity of the deteriorated girder. In a recent study by Wu et al. (2018) the deteriorated beam was strengthened by welding stiffeners on the two sides of the web, and then partially encasing it with high-strength grout.

For MassDOT engineers, the current procedure to estimate the remaining capacity of corroded unstiffened girder ends is included in Mass LRFD Manual (MassDOT 2018). The capacity is considered as the minimum of yielding and crippling resistance of a defined area of interest. The crippling capacity is determined by following the work of Roberts et al. (1981) who proposed the plastic hinge failure mechanism for stiffened beams subjected to edge loading. His work was both experimental and theoretical but according to other researchers it may be inaccurate for unstiffened sections (Kayser et al. 1989).

The present paper is part of ongoing investigation that aims to develop procedures for determining the safe capacity of unstiffened deteriorated beams, which constitute the majority of deteriorated bridges in Massachusetts. In this framework two beams with extensive end corrosion are tested. Due to the fact these girders were removed from an in-service bridge, the need for artificial corrosion was precluded. The exact experimental configuration is simulated using Finite Element Method, and the model is calibrated using the experimental data.

2. Experimental Program
This section describes the procedure for selecting specimens, the experimental and instrumentation configuration as well as the experimental results obtained by the testing of two girders with natural corrosion.

2.1 Test Specimens
At the time this research project began, a bridge rehabilitation project was in progress in the state of Massachusetts. In particular, a five span bridge in Colrain, MA, was under deconstruction (Structure ID: C18028-0KQ-DOT-NBI). The structure connects Route MA-112 over the East Branch of the North River. The Colrain bridge was built in 1933 as a three spans bridge consisting of five continuous riveted steel plate girders. Later on, the bridge was rebuilt with the addition of one span to each end. The additional spans employed simply supported unstiffened rolled steel beams.

The research team visited the construction site, which at the time, already had the west half of the structure removed. However, the beams remaining on the east half had experienced visibly significant deterioration, and spanned 50 feet. As such, some of them met the standards for the scope of the current research project. Before transporting the specimens to UMass, it was decided the best practice would be to cut the beams in half. The advantage of this was two-fold. First, it provided ease of transport. Second, it would allow both beams to be in compliance with laboratory length restrictions.

While the bridge was in service, a concrete diaphragm was located above the support. During the bridge deconstruction, the concrete was removed, while the steel angle sections remained bolted

to both sides of the web. The beams were delivered to UMass testing facility with the bearing plate still welded to the girder's end. The anchors protruding from the bottom of the bearing had to be sawn off.

The first specimen is a 332'' long 33WF125 with extensive end corrosion. The most extensive section loss was observed in the lower half of the web. Two holes could also be observed among the corrosion, Fig. 1a. The first one (6 inches long x 0.5 inches high) was located directly above the flange. At the inner perimeter of the hole, the web had crippled in a distance of 3 inches along the longitudinal axis of the beam. The second area with 100% section loss (3 inches long x 2 inches high) was located below the steel section angles.
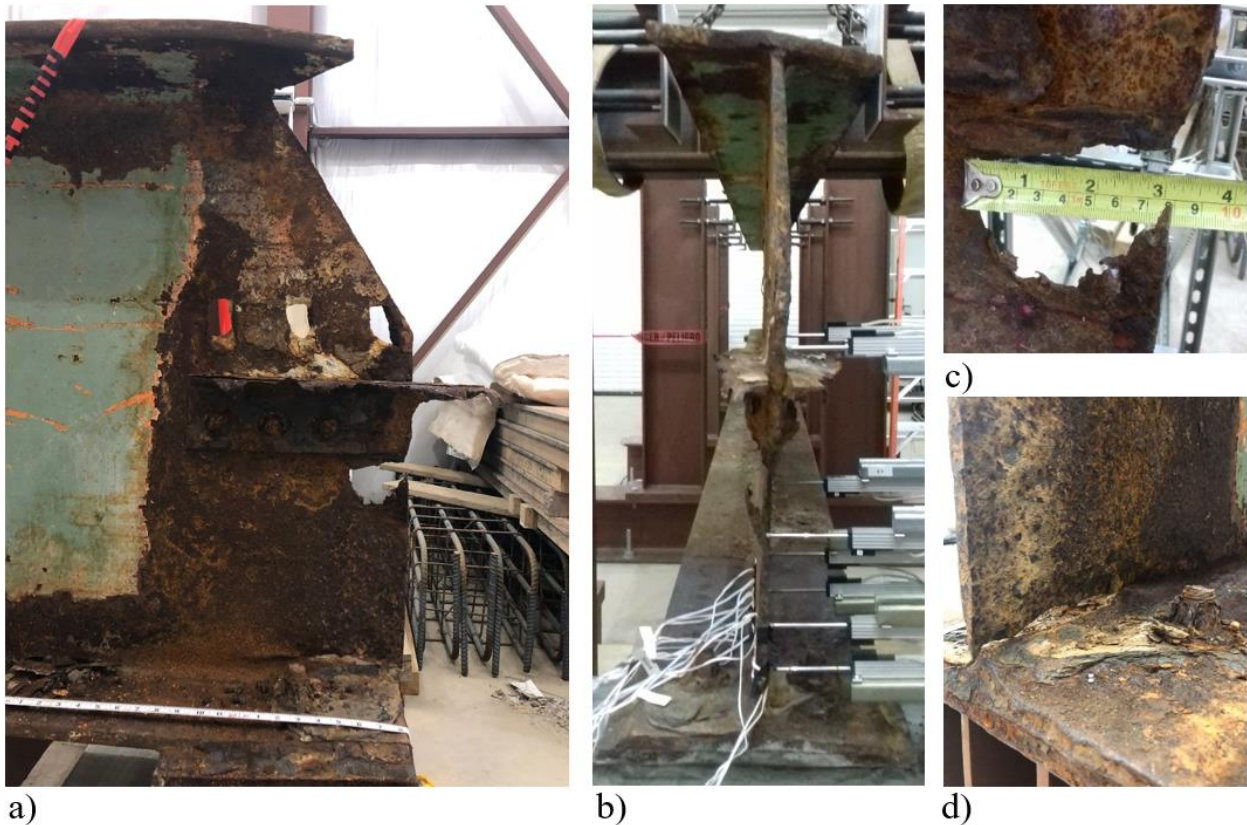

a) b) d)

Figure 1: a) Side and b) front view of the corroded end of specimen 1. Area with 100% section loss c) below the steel section angle and d)above the flange as it looked from the web side. At the inner end of the hole the web had crippled in a distance of 3 inches along the longitudinal beams axis.

Specimen 2 is a 286.5'' long 33WF132 girder. The most extensive section loss in the web was observed in three different areas above the support. The first distinct area is located parallel to the inner edge of the concrete diaphragm. This topology reveals a likelihood that water consistently flowed from the top of the beam to the bottom flange following this path. The second area of distinct section loss proceeds diagonally across the web between the steel angle sections and the bottom flange. Finally, the last distinct area is a five-inch-long by 1-inch-high area at the bottom of the web. It should be also mentioned that there is a small hole located below the steel angle sections. The defining feature of specimen 2 is its extensive initial lateral web displacement which reaches 1.58''.

Figure 2: a) The corroded end of specimen 2 b) The maximum initial lateral displacement equals to 1.58'' c) The two areas with extensive section loss at second's specimen web d) A quarter inch diameter hole, located 4 inches below the steel angle sections.

2.2 Experimental Configuration

The experimental test setup was designed to fully restrict and safely apply loading to failure of test girder specimens. The test setup ensures that the failure mode occurs in the corroded region of interest, therefore a lateral restricting system was designed using a cantilevered W-section with bolted C-channel arms. These restriction devises were placed at 4 locations along the test specimen. The first brace was placed close to the corroded end, to help with its stability, and then every 5 ft after the cross beam to ensure the limit state of lateral torsional buckling does not exist.

The loading configuration consists of two, 60-ton through-hole jacks applying load to the top flange through the cross beam. The cross beam was designed as two separate W-sections welded together to allow passage of a threaded rod that is anchored to the strong floor. Fig. 3a shows a physical representation of the lateral torsional buckling restraints as well as the instrumentation configuration, and Fig. 3b shows the design of the loading configuration.

It is considered also critical to identify the exact reaction force conveyed through the support at the corroded end during the experimental process, as well as the failure load. The equipment used to perform the tests allowed for control of the applied load. Two, 200 lb through hole load cells were placed at the anchorage point of the threaded rods, while a third compression load cell was placed at the intact end of the specimen. Based on force equilibrium at the rods, the summation of the recorded tension forces is equal to the total applied load, while the force

recorded by the compressive load cell would yield the reaction at the point. Again based on force equilibrium, the reaction force at the corroded end could be determined by calculating the difference between the applied downward load and the intact bearing upward reaction force. The maximum beam deflection was measured using a linear variable displacement transducer (LVDT) installed on the bottom face of the bottom flange, beneath the point of load application.
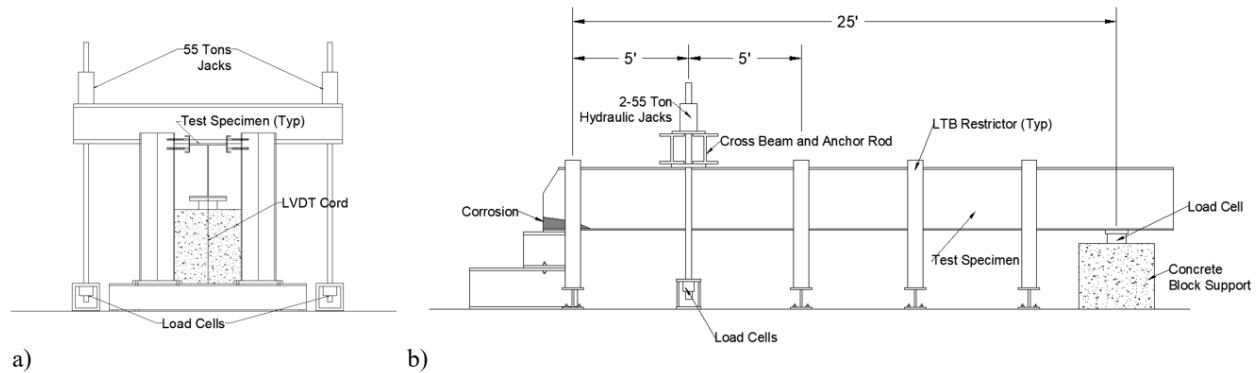

Figure 3: Representation of experimental and instrumentation configuration. a) Typical Lateral Torsional Buckling restrain system for test specimens, as well as Load cells and LVDT configuration for the monitoring of the applied load, reaction forces as well vertical displacement b) side view of completely restrained test specimen and loading configuration.

2.3 Test Results

According to the summation of the reaction forces measured in the two load cells installed at the bottom end of each rod, the total applied load at failure was equal to 134.08 kips for specimen 1 and 99.3 kips for specimen 2. Subtracting the part of the load that was distributed to the intact ends, the capacities of the corroded ends were calculated equal to 99 kips and 67.6 kips respectively.
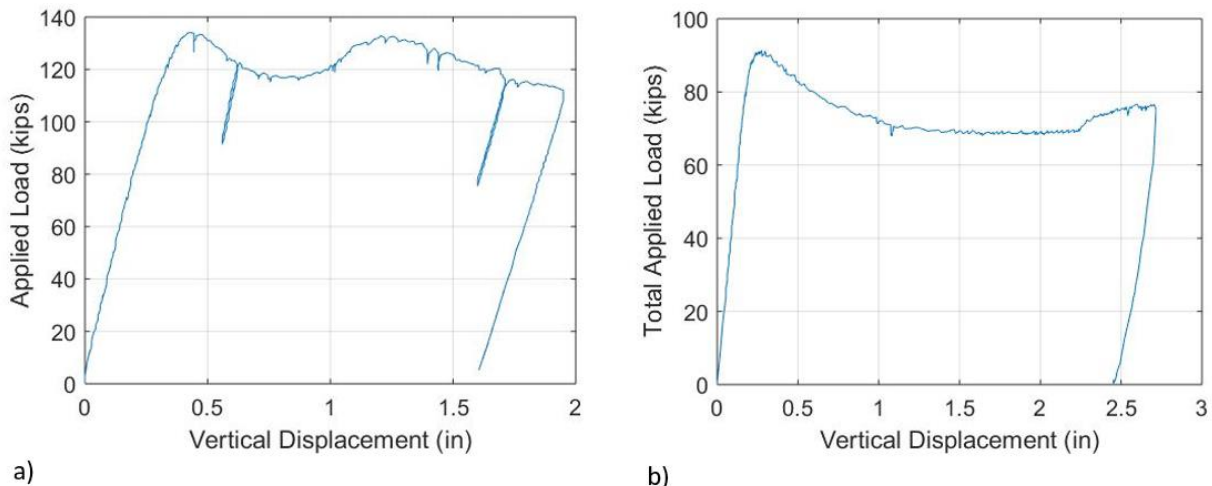

Figure 4: Applied load vs vertical displacement plot for a) specimen 1 and b) specimen 2. The peak load equals to 134.08 kips for specimen 1 and 99 kips for specimen 2. The beam deflection was measured using a LVTD device installed bellow the outer face of the bottom flange beneath the point of load application.

For both specimens, after the peak load has been reached, the undertaken load is reducing with increasing displacements. No sudden collapse is observed and failure occurs gradually for both girders. The applied load, after peak, initially plateaus and unexpectedly the specimens gain stiffness. For specimen 1, Fig. 4a, the reason of the sudden load rise is that the deformed web, above the bottom web hole, started bearing on the bottom flange retaining additional load. For specimen 2, this behavior can be attributed to the web bearing on the top of the anchor protruding from the flange. At both cases, the loading was terminated when the vertical displacement capacity of the lateral support was reached.

3. Computational Model
The first step of a problem formulation is to accurately describe the mechanical model in terms of its geometry, boundary and loading conditions. In this section, each one of these aspects are described in detail. Finally, the Finite Element Method is used to capture the failure load and mode of the corroded end.

3.1 Mechanical Model
Both boundary and loading conditions simulate the exact experimental configuration. In particular the load is applied as uniform pressure in the location of the loading plate. The loading plate covers the full flange width and its length equals to 18 inches. The out of plane displacement is not allowed at the locations of the LTB restrictions. The bottom flange of the girder is resting on two steel bearing plates, which are considered fixed.

Concerning the section loss, except for the areas with 100% thickness loss, it is necessary to define the thickness reduction profile along the corroded end. In this framework, detailed thickness measurement were obtained. The data was gathered using a Pocket MIKE Compact Thickness Gauge manufactured by GE Inspection technologies. This device provided display resolution of 0.001in for any material thickness up to 10 inches (GE Inspection Technologies 2004). For specimen 1, 159 points were measured on the web and 42 points at the bottom flange. For specimen 2, 183 points were measured at the web and ten at the bottom flange.

For ease of reference, a grid was drawn, covering the full depth of the web and two feet along the length of the beam. Moving from top to bottom, the grid increases in resolution, as visual inspection indicates the section loss to be most severe towards the bottom flange. The top row of segments are $16in^2$ boxes, which transitions to $4in^2$, and finally $1\ in^2$ boxes at the bottom of the web. Fig. 5 illustrate the exact points at which the thicknesses were measured.

In order to replicate the thickness reduction distribution along the corroded end, points with common or similar thickness loss were grouped together forming areas with uniform thickness reduction. An approach of simulating the corrosion topology is illustrated at Fig. 5 for specimens 1 and 2.

Finally, the last aspect of the geometry description, is the initial out of placement displacement of the web. In this framework, each model was initially run using an eigenvalue buckling analysis solver. The eigenmode which was closer to the actual deformation of the beam was imported as an imperfection for the quasi-static analysis scaled to the actual lateral deflection.

7

To determine the material properties of the steel girder, four 22"x5" steel plates were cut out of the steel girder from various locations, the number of test coupons as well as, their location were derived from ASTM Standard E8 (ASTM 2011). On each plate dogbone shaped coupons were cut out and tested.
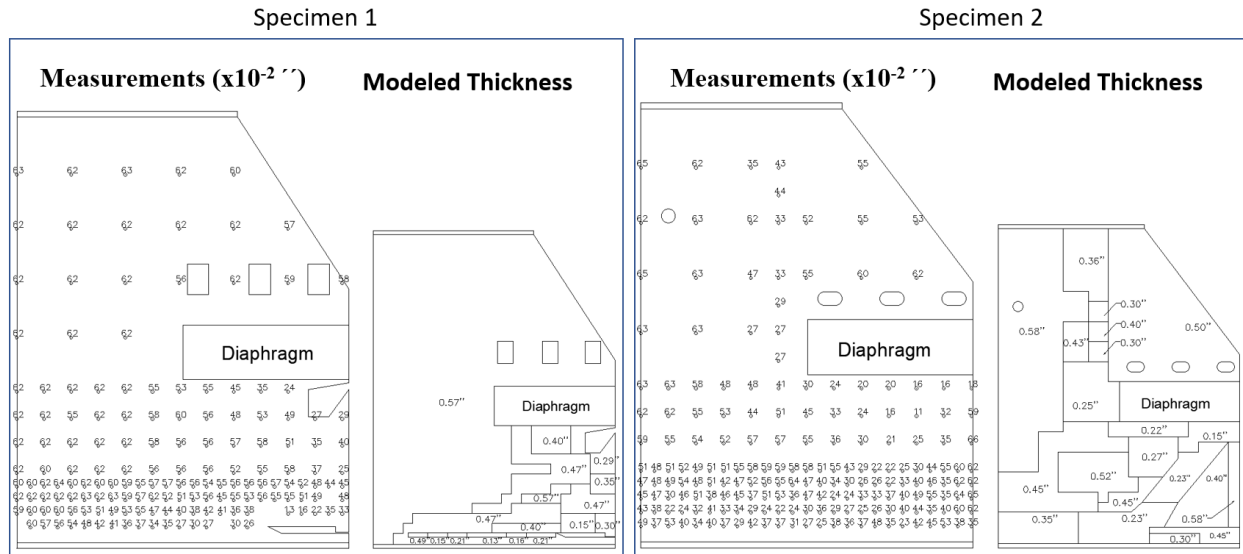

Figure 5: Illustrates the taken thickness measurements along both specimens. Points with common or similar thickness loss were grouped together forming areas with uniform thickness reduction. The intact web thickness is 0.57'' for specimen 1 and 0.58'' for specimen 2.

3.2 Finite Element Procedures

The specimen was modeled using the finite element software package ABAQUS (Simulia, 2014). The girder was simulated with a mid-surface shell model. Both the web and flange thicknesses are assigned to the corresponding shell elements. The remaining thickness is simulated by assigning a uniform reduced thickness at the elements located in the deteriorated area. Holes are simulated with lack of elements.

The interaction between bottom flange and bearing plate is simulated with "softened contact". The contact interaction is defined using a linear contact pressure-overclosure relationship. The contact algorithm in Abaqus does not take into account material, section or other properties to automatically calculate the contact pressure-overclosure, but the user needs to define the slope of the linear relationship, "k". The "k" value is defined using the experimental data.

Except for contact properties defined on the normal direction between the bottom flange and the bearing plate, a penalty friction is defined to simulate the interaction between the bottom flange and the bearing plate in the tangential direction. In order to define a correct friction coefficient value, a sensitivity analysis was performed. The analysis was consecutively performed for friction coefficients in the range of {0.5, 0.55, 0.6, 0.65, 0.7, 0.75, 0.8, 0.85, and 0.9}. The beam capacity seemed to be only slightly affected by the contact coefficient variation. The maximum divergence among the results is 1.2%. A contact coefficient equal to 0.74 was selected for the rest of the work.

8

Computational time is an important aspect of this research because thousands of analyses will be performed. To limit the computational time while ensuring the accuracy of the results and the ability of the model to capture all failure modes, a mesh convergence study was performed. Equal sized S4R elements are used. At midspan the element size is 2 inches. At the beam ends, where stress concertation and the failure are expected to occur, a denser mesh area was defined. This area covers the full height of the web and its length exceeds the corrosion length by 5 inches. For this area the element size is 0.5 inches.

Contact interaction can potentially be sensitive also to the load increment used in a quasi-static analysis framework. In order to validate analysis against this kind of sensitivity, an increment convergence is also performed. In conclusion, analyses will be performed using the following loading-increment sizes: Initial 0.001, Minimum 1x10-15, Maximum 0.01.

3.3 Computational Results
Following the procedure described in the previous section and using contact stiffness "k" equal to 10, the applied load – vertical displacement curve is plotted to compare the finite element with the experimental results for both specimens. The maximum beam deflection was measured using a linear variable displacement transducer (LVDT) installed on the bottom face of the bottom flange beneath the point of load application.

As it has been already mentioned quasi-static analysis was performed. Quasi-static analysis is not able to capture post buckling behavior, which is the reason that the FEM curves are terminated at the point of peak load as this is done automatically by the numerical analysis.

Fig. 6 indicates that the computational model is able to capture the failure load as well as the stiffness of the specimen. For the first specimen the difference between the numerically calculated applied load and the experimental one is -1.7% (Experimental: 134.08 kips, FEM: 131.7 kips), while for specimen 2 the computational model overestimates the load for 2.9% (Experimental: 91.3 kips, FEM: 93.97 kips).
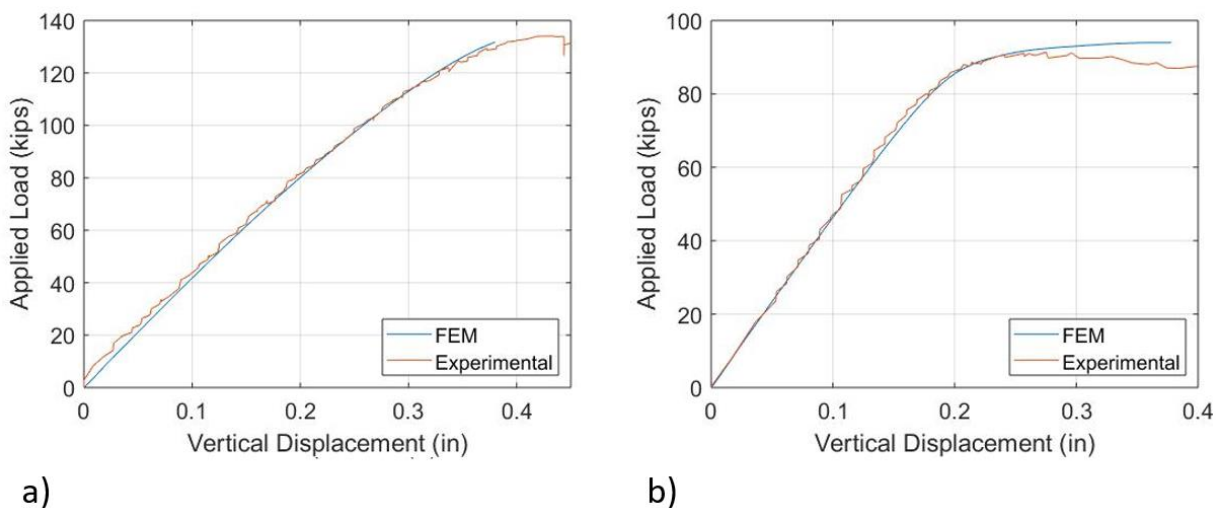

Figure 6: Comparison of experimental and numerical results for a) specimen 1 and b) specimen 2

9

Except for the failure load Fig. 7 indicates that the developed computational model is also able to capture the failure mode. In detail, Fig. a, d and b, e present the failure mode obtained from the experiment and the computational model respectively for the two specimens. Figure 8c and 8f show the relation of load versus lateral deformation for both specimens and the associated computational nodal displacements.
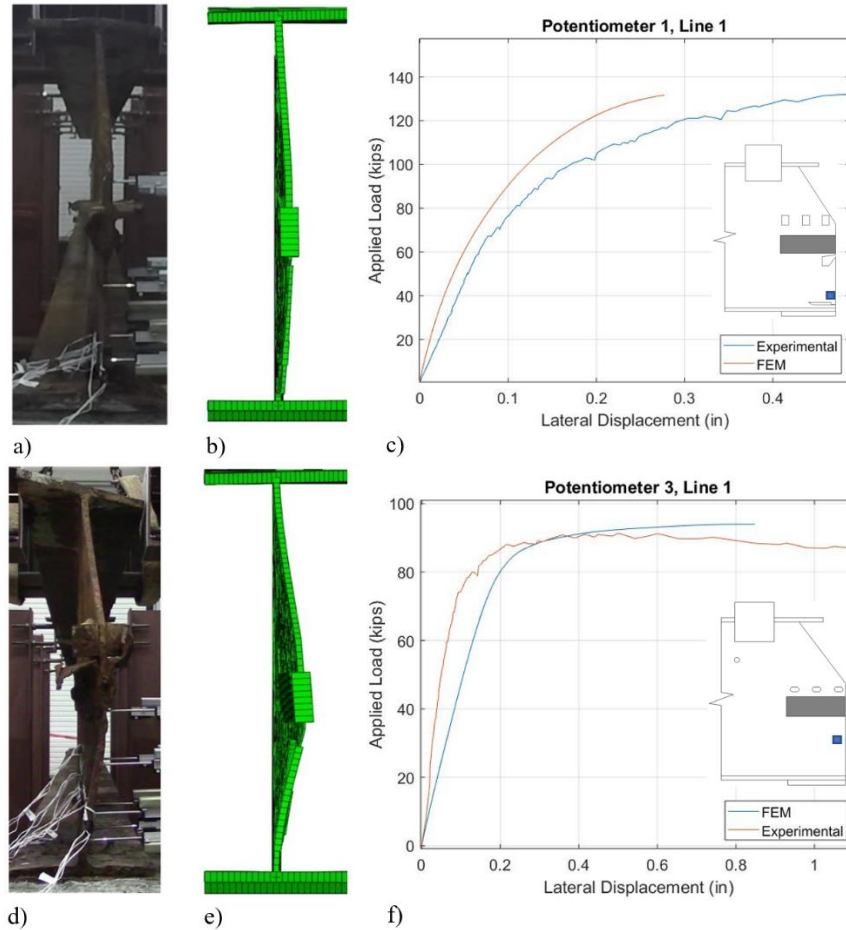

Figure 7: Failure mode for a) specimen 1 and d) specimen 2. Deformations at peak loads according to FEM b) for specimen 1 and e) specimen 2. Comparison of experimentally and computationally obtained later displacements for c) specimen 1 and f) specimen 2.

The developed model seems to capture more satisfactorily the lateral displacement of specimen 2 compared to specimen 1. However, this is not particularly surprising given the fact that the imported imperfection of specimen 1 was not able to mimic the exact lateral deflection profile of the web above the bottom hole. This discrepancy resulted in a reduction of the out of plane displacement for the computational model compared to the experimental one. Simultaneously, this behavior indicates the sensitivity of the model in terms of its geometry.

Considering the variability of the thickness reduction along the corroded end, as well as the difficulty to simulate the initial geometric imperfection of the girders using shell elements, the presented results prove the detailed work conducted to simulate the initial condition of the specimens.

4. Current Procedures Evaluation

Before proceeding with the development of new procedures for deteriorated beam capacity, it is critical to evaluate the current MassDOT procedures. Having surveyed both specimens section loss, it is possible to calculate the remaining capacity following the recommendations of Section 7.2.8 of the MassDOT LRFD Bridge Manual (MassDOT 2018).

The factored corroded web resistance is calculated as the minimum of the yielding ($R_{n,yield}$) and crippling ($R_{n,crip}$) capacity based on the equation below:

$$\text{Corroded Web Factored Resistance} = [\text{R}_{n,yield}, 0.8\,\text{R}_{n,crip}] \tag{1}$$

For the tested specimens the nominal yielding capacity is calculated as follow:

$$R_{n,yield} = F_y t_{ave}(2.5k + N) \tag{2}$$

Where F_y is the minimum yield strength, t_{ave} the average remaining thickness within the bottom 4'' of the web height and k the distance from outer face of flange to web toe fillet. Finally, the web local crippling capacity in kips ($R_{n,crip}$) is calculated as follows:

$$R_{n,crip} = 0.4t_{ave}^2 \left[1 + \left(\frac{4(N-H)}{d} - 0.2\right)\left(\frac{t_{ave}}{t_f}\right)^{1.5}\right]\sqrt{\frac{EF_y t_f}{t_{ave}}} \tag{3}$$

Where d is the entire depth of steel section, t_f is thickness of the flange resisting the bearing reaction and E the modulus of elasticity of steel. The average remaining web thickness is calculated as follow:

$$t_{ave} = \frac{(N+2.5k-H)*t_w}{(N+2.5k)} \tag{4}$$

Where t_w is the remaining web thickness, H the length of hole along length used for capacity, N the bearing length and k the distance from outer face of flange to web toe fillet.

Both capacities (crippling and yielding) are dependent on t_{ave} (the average remaining thickness within the bottom 4'' of the web). t_{ave} is calculated using Eq. 4, where the inspection engineer has to input the remaining web thickness. Given the fact, that section loss is not uniform along this area, the calculated capacity is heavily dependent on engineering judgement regarding the remaining thickness estimation. In the framework of our calculations, the weighted average of the thickness measurements illustrated in Fig. 5 are used to estimate the remaining thickness in the area of interest.

For the calculation of capacities for both specimens the nominal material and section properties have been used. In details, 36 ksi steel was considered, with Young's modulus equal to 29,000 ksi. The first specimen is a 33WF125 with one hole (6 inches long x 0.5 inches high) in the bottom 4'' of the web. By setting $t_w = 50\%\ t_{web,intact}$ and $H=6''$, the Corroded Web Resistance was found 23 kips, on the other hand the experimental capacity is 99 kips.

The second specimen is a 33WF132 beam. Given the section properties and absence of sections with 100% material loss the remaining web thickness was considered as, $t_w=50\%t_{web,intact}$, and the Corroded Web Resistance was calculated equal to 58.9 kips, while the experimental capacity is 67.6 kips.

5. Conclusions

The work presented an ongoing investigation that aims to develop procedures for determining the safe capacity of unstiffened deteriorated beams. Two girders with natural corrosion were obtained from a bridge undergoing replacement and tested in the UMass Amherst Brack Structural Testing Laboratory. The most striking result to emerge from this test is that for specimen 1 the current MassDOT procedures underestimated the capacity of the corroded end by 3.3 times compared to the experimentally obtained capacity. On the other hand, for specimen 2 the nominal capacity is in good agreement with the experimental one. The experimental data was used to calibrate a Finite Element Model able to capture the behavior of the specimen in terms of its stiffness, as well as failure mode and load. Finally, the finite element model will be used to investigate the effect of the most common corrosion topologies, which the research team has already identified but are not presented in the framework of this paper.

References

AASHTO (2012). "LRFD bridge design specification." Washington, DC. Association of State Highway and Transportation Officials.

Ahn, J.H., Kainuma, S., Kim, I.T. (2013a). "Shear failure behaviors of a web panel with local corrosion depending on web boundary conditions." *Thin-Walled Structures*, 73 302-317.

Ahn, J.H., Kim, I.T., Kainuma, S., Lee, M.J. (2013b). "Residual shear strength of steel plate girder due to web local corrosion." *Journal of Constructional Steel Research, 89 198-212.*

Ahn, J.H., Kainuma, S., Yasuo, F., Takehiro, I. (2013c). "Repair method and residual bearing strength evaluation of a locally corroded plate girder at support." *Engineering Failure Analysis,* 33 198-418.

Ahn, J.H., Cheung, J.H., Lee, W.H., Oh, H., Kim, I.T. (2015). "Shear buckling experiments of web panel with pitting and through- thickness corrosion damage." *Journal of Constructional Steel Research,* 115 290-302.

ASCE (2017). "Report card for America's infrastructures." https://www.infrastructurereportcard.org/wp-content/uploads/2017/01/Bridges-Final.pdf.

ASTM Standard E8/E8M (2011). "Standard test methods for tension testing of metallic materials." West Conshohocken, PA. ASTM International.

FHWA (2017a). "National bridge inventory database." Accessed July 21, 2017. https://www.fhwa.dot.gov/bridge/nbi/no10/defbr17.cfm.

FHWA (2017b). "National bridge inventory database." Accessed July 21, 2017. https://www.fhwa.dot.gov/bridge/nbi/no10/yrblt.pdf.

Gheitasi, A., Harris, D. (2015). "Redundancy and Operational Safety of Composite stringer bridges with deteriorated girders." *Journal of Performance of Constructed Facilities.*

Kayser, J.R., Nowak, A.S. (1989). "Capacity loss due to corrosion in steel-girder bridges." *Journal of Structural Engineering,* 115 1525-1537.

Koch, G.H., Brongers, M.P.H., Thompson, N.G., Virmani, Y.P., Payer, J.H. (2002). "Corrosion cost and preventive strategies in the United States." Turner-Fairbank Highway Research Center.

Khurram, N., Sasaki, E., Katsuchi, H., Yamada, H. (2014). "Experimental and numerical evaluation of bearing capacity of steel plate girder affected by end panel corrosion." *International Journal of Steel Structures*, 14 659-676.

Kim, I.T., Lee, M.J., Ahn, J.H., Kainuma, A. (2013). "Experimental evaluation of shear buckling behaviors and strength of locally corroded web." *Journal of Constructional Steel Research,* 83 75-89.

Liu, C., Miyashita, T., Nagai, M. (2011). "Analytical study on shear capacity of steel I-girders with local corrosion nearby supports." *Procedia Engineering,* 14 2276-2284.

MassDOT. "LRFD bridge manual part I." Boston, MA. The Massachusetts Department of Transportation Highway Division Bridge Section.

Miyashita, T., Nagai, M., Wakabayashi, D., Hidekuma, Y., Kobayashi, A., Okuyama, Y., Koibe, N., Horimoto, W. (2015). "Repair method for corroded steel girder ends using CFRP sheet." *Proceedings of IABSE – JSCE Joint Conference on Advances in Bridge Engineering- III*, Bangladesh.

Ogami, H., Fujii, K., Yamada, T., Iwasaki, H. (2015). "Renovation of corroded girder end in plate girder bridge with resin and rebars." *Implementing Innovative Ideas in Structural Engineering and Project Management*.

PocketMIKE (2004). "Operating manual." GE Inspection Technologies, Lewistown, PA.

Roberts, T.M. (1981). "Slender Plate Girders Subjected to Edge Loading." *Proceedings of the Institution of Civil Engineers Part B,* 71 805-819.

Simulia (2014). "ABAQUS theory manual, v.6.14" Dassault Systems Simulia Corporation, Providence, RI.

Sugimoto, I., Kobayashi, Y., Ichikawa A. (2006). "Durability evaluation based on buckling sharacteristics of corroded steel deck girders." *Quarterly report of Railway Technical Research Institute*, 47 150-155.

Usukura, M., Yamaguchi, T., Suzuki, Y., Mitsugi, Y. (2013). "Strength evaluation for a corroded damaged steel girder end considering its collapse mechanism." *Proceedings of the 13th East Asia-Pacific Conference on Structural Engineering and Construction (EASEC).*

Van de Lindt, J.W., Ahlborn, T.M. (2013). "Development of Steel Beam End Deterioration Guidelines." Publication MDOT-RC-1454, Michigan Tech Transportation Institute.

Wu, B., Cao, J.L., Kang L. (2018). "End patch loading behavior and strengthening of locally corroded steel I-beams." *Journal of Constructional Steel Research,* 148 371-382.

Yamaguchi, E., Akagi, T. (2013). "Degradation of load- carrying capacity of steel I- girder end due to corrosion." *Proceedings of the 13th East Asia-Pacific Conference on Structural Engineering and Construction (EASEC).*

Zmetra, K.M., McMullen, K.F., Zaghi, A.E., Wille K. (2017). "Experimental study of UHPC repair for corrosion-damaged steel girder ends." *Journal of Bridge Engineering,* 22.